QUANTUM CHAOS: FROM SIMPLE MODELS TO QUANTUM COMPUTERS

Dima Shepelyansky

http://www.quantware.ups-tlse.fr

CNRS, Toulouse, France

- Kolmogorov complexity, classical chaos (Arnold cat map, Chirikov standard map)
- Quantum chaos in one-body systems (kicked rotator, Rydberg and cold atoms, rough billiards, ...)
- Quantum chaos in many-body systems (complex nuclei, atoms, quantum dots, quantum computers)
- Quantum computers gambling chaos

Supported by EU TMR Program and NSA/ARO contract

Arnold cat map

$$\bar{x} = x + y \qquad \bar{y} = x + 2y \quad (\mathrm{mod}\ 1)$$

$$h = \ln\left(\frac{3+\sqrt{5}}{2}\right) \approx 1 > 0$$

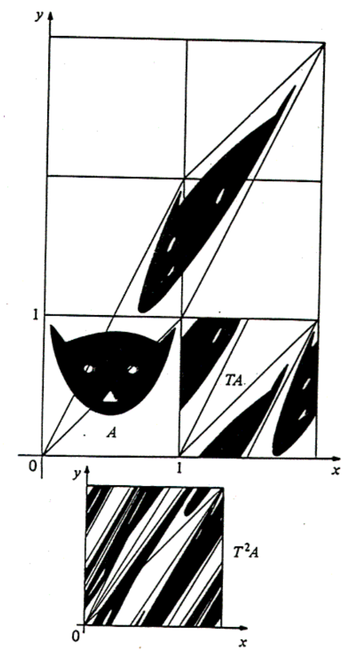

Arnold's cat mapping, showing the cat A transformed to TA and to T^2A. This is a C-system (after Arnold and Avez, 1968).

$$\Delta x(t) \approx e^{ht} \Delta x(0)$$

$$\Delta x(0) \sim 10^{-16} \rightarrow t \approx 38$$

Pentium III

F1

The Chirikov Standard Map

$$\bar{y} = y + \frac{K}{2\pi} \sin(2\pi x)$$
$$\bar{x} = x + \bar{y}$$

$$K_g = 0,971635406 31$$

$$r_g = \frac{x_n - x_0}{n} = \frac{\sqrt{5}-1}{2} = [1,1,1 \ldots]$$

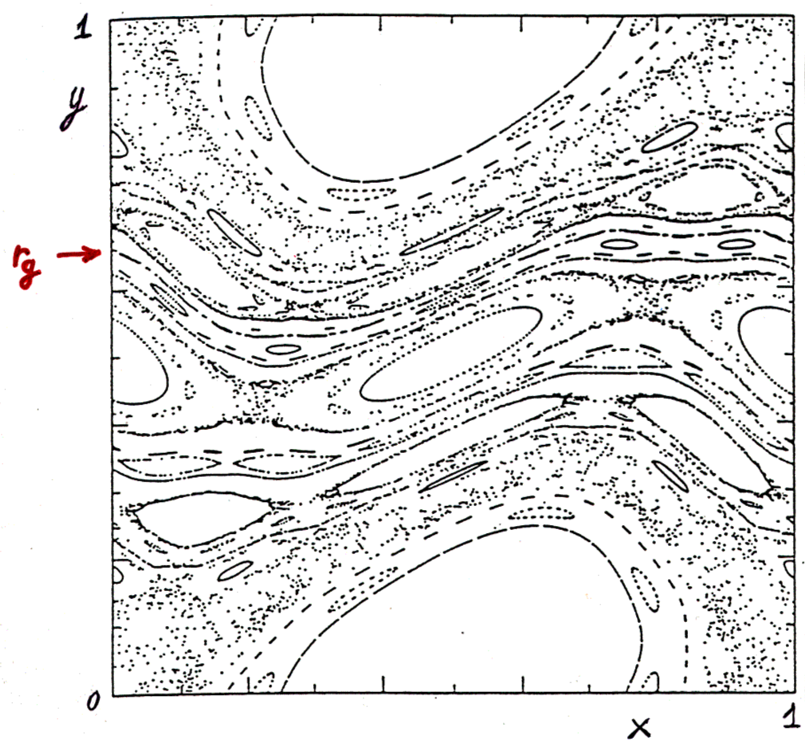

KICKED ROTATOR

Classical kicked rotator (Chirikov standard map)

$$\boxed{\begin{aligned} \bar{n} &= n + k \sin\theta \\ \bar{\theta} &= \theta + T\bar{n} \end{aligned}}$$

The system dynamics depends only on $K = kT$

$K \ll 1$ KAM integrability

$K \gg K_g \approx 0.97 \Rightarrow$ chaos, classical diffusion of n

Positive Kolmogorov-Sinai entropy

$h \approx \ln(K/2) > 0 \ \ (K > 4)$.

In the chaotic component classical diffusion takes place for $K > K_g$ with the rate D $(n^2 \approx Dt)$ which can be approximated by

$$\begin{aligned} D &\approx \frac{k^2}{2} \text{ for } K > 4.5 \\ &\approx \frac{(K-K_g)^3}{3T^2} \text{ for } K_g < K < 4.5 \end{aligned}$$

Casati, Chirikov, Ford, Izrailev (1979)

Quantum kicked rotator, with the Hamiltonian

$$\hat{H} = \frac{\hat{n}^2}{2} + k\cos\hat{\theta} \cdot \sum_m \delta(t - mT)$$

The evolution operator is

$$\boxed{\hat{U} = e^{-ik\cos\hat{\theta}}\, e^{-iT\frac{\hat{n}^2}{2}}}$$

Here $\hbar = 1$, $\hat{n} = -i\ d/d\theta$ and the classical limit corresponds to $k \gg 1, T \ll 1, K = kT = const.$

Quantum interference leads to localization of chaotic diffusion after diffusive time scale

$$\boxed{t^* \approx D \approx k^2/2 \propto 1/\hbar^2}$$

This scale is much larger than the Ehrenfest time scale

$$\boxed{t_E \approx \ln k/h \ll t^*}$$

on which the minimal coherent wave packet is spreaded over classical cell.

The eigenstates are exponentially localized with localization length

$$\boxed{l \approx D/2 \approx k^2/4 \approx t^*/2}$$

$\bar{n} = n + k\sin\theta,\ \bar{\theta} = \theta + T\bar{n}$ D. S. (1983)

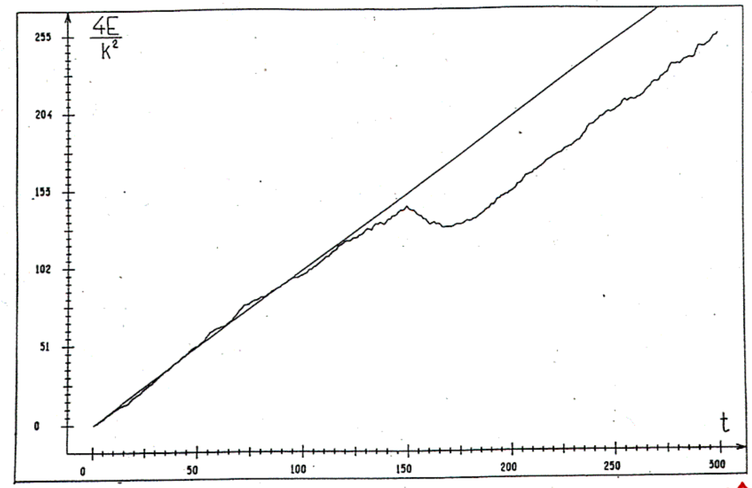

classical ↑

Chirikov standard map
$K = kT > 1$

quantum ↓

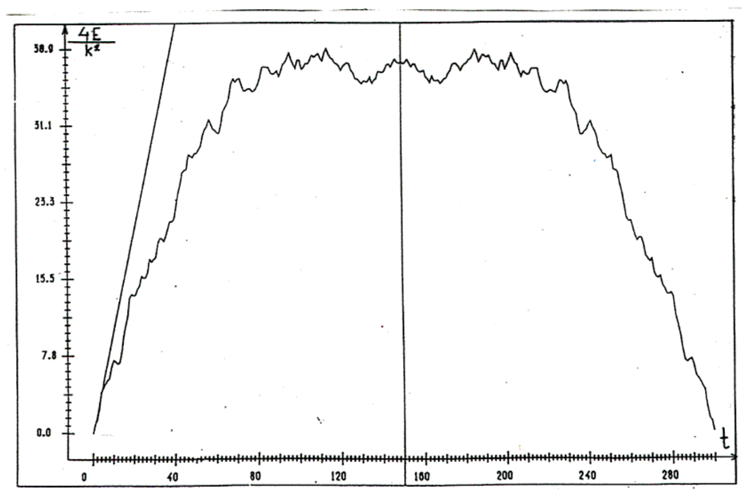

$K = 5$
$k = 20$

↑ time reversion

computer precision 10^{-12}

VOLUME 75, NUMBER 25 PHYSICAL REVIEW LETTERS 18 DECEMBER 1995

Atom Optics Realization of the Quantum δ-Kicked Rotor

F. L. Moore,* J. C. Robinson, C. F. Bharucha, Bala Sundaram, and M. G. Raizen
Department of Physics, The University of Texas at Austin, Austin, Texas 78712-1081
(Received 21 July 1995)

We report the first direct experimental realization of the quantum δ-kicked rotor. Our system consists of a dilute sample of ultracold sodium atoms in a periodic standing wave of near-resonant light that is pulsed on periodically in time to approximate a series of delta functions. Momentum spread of the atoms increases diffusively with every pulse until the "quantum break time" after which exponentially localized distributions are observed. Quantum resonances are found for specific values of the pulse period.

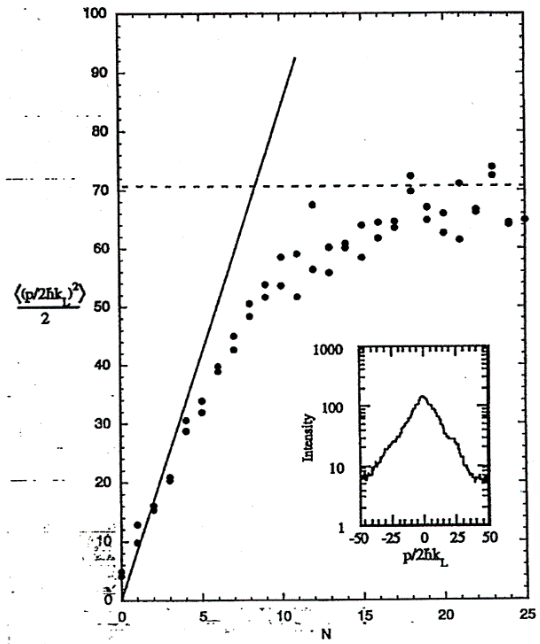

FIG. 4. Energy $\langle (p/2\hbar k_L)^2 \rangle/2$ as a function of time. The solid dots are the experimental results. The solid line shows the calculated linear growth proportional to the classical diffusion constant $\kappa^2/2$. The dashed line is the saturation value computed from the theoretical localization length ξ. The inset shows an experimentally measured exponential line shape on a logarithmic scale which is consistent with the prediction $\xi = \kappa^2/4k^2 \approx 8.3$.

K. Frahm, D. S. (1997)

Quantum chaos in rough billiards

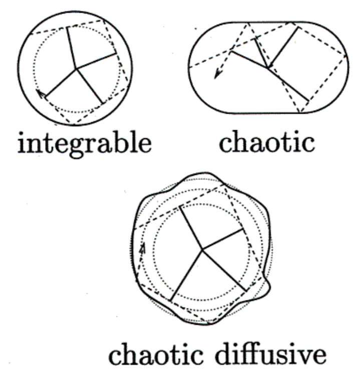

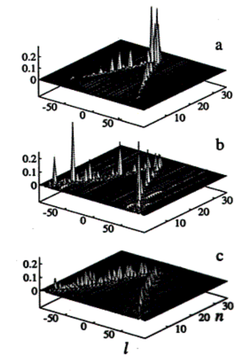

Classical problem: diffusion in angular momentum space

$\boxed{\Rightarrow t_{\text{ergodic}} \gg t_{\text{collision}}}$

Quantum problem: Floquet operator

$$\boxed{S_{l,\tilde{l}} = e^{i\mu_l + i\mu_{\tilde{l}}} \ < l|\exp[ik\Delta R(\theta)]|\tilde{l} >}$$

$\rightarrow$ quantum localization and Breit-Wigner regime.

(Microwave experiment by Stöckmann et al.)

Transition from localisation to Shnirelman ergodicity

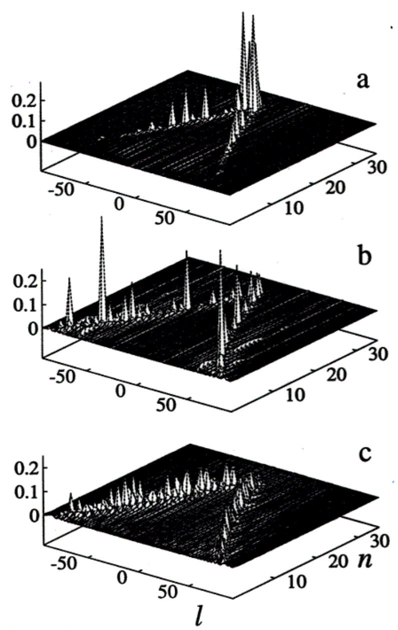

Energy surface for level number $N \approx 2250$, $l_{max} \approx 95$ and $M = 20$; shown are the absolute amplitudes $|C_{nl}^{(\alpha)}|$ of one eigenstate: (a) localization for $D(l_r = 0) = 20$; (b) Wigner ergodicity for $D = 80$; (c) Shnirelman ergodicity for $D = 1000$.

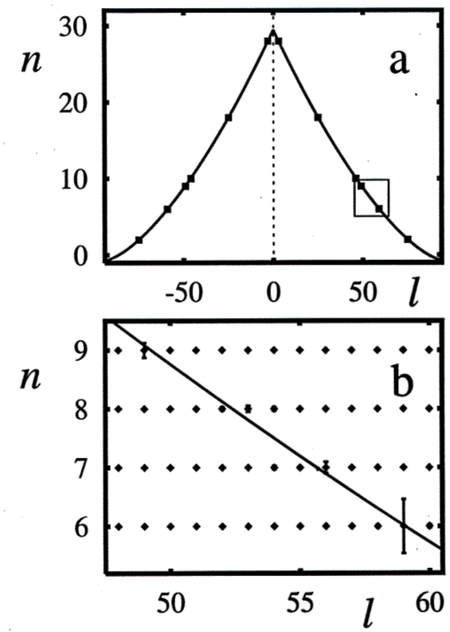

(a) Main peaks of eigenstate in case (b) (squares for $|C_{nl}^{(\alpha)}| \geq 0.1$) shown on the energy surface $\mathcal{H}(n,l) = E_\alpha$; (b) rescaled part of (a): diamonds show the integer (n,l)-lattice, the errorbar size is $2|C_{nl}^{(\alpha)}|$.

Mixing of multi-qubit levels by inter-qubit interaction

Δ_0 – one-qubit spacing

$N = 2^n$ – size of Hilbert space

$B = n\Delta_0$ – multi-qubit energy band

$\Delta_n = \frac{B}{N} = \frac{n\Delta_0}{2^n}$ – average multi-qubit level spacing

J – residual interqubit coupling

$\boxed{J \gg \Delta_n}$? naive expectation

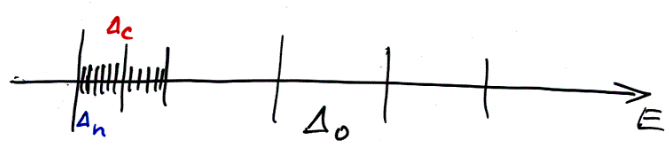

Example: $n = 1000$ (as in Shor algorithm)

$\Delta_0 \sim 1\ K \Longrightarrow \Delta_n \sim 10^{-298}\ K$

$J \sim \Delta_0 \propto \exp(-R/a_B^*)$ qubit → nuclear spin

$J \sim \Delta_0 \sim 1\ K$ $(R \sim 200\ \text{Å},\ a_B^* \sim 30\ \text{Å})$

Kane (1998)

$a_B^* \propto \frac{1}{m^*} \rightarrow \frac{1}{2} a_B^*$

$\Longrightarrow$ $\boxed{J \sim 10^{-5}\ K \gg \Delta_n \sim 10^{-298}\ K}$

Real border: $\boxed{J_c \approx \frac{3\Delta_0}{n} \sim 1\ mK}$

Georgeot, D.S. (1999)

Åberg Criterion for quantum chaos in many-body systems

Wigner (1951-57)

Random matrix theory

Two-body nature of interaction (TBRIM)

French, Wong (1970-1971)

Bohigas, Flores

strong interaction limit $\Longrightarrow$ RMT

Weak interaction?

Åberg (1990)

$U_c \sim \Delta_c$

interaction matrix element

spacing between directly coupled states

Åberg criterion:

different independent confirmations

- 3 particles with random 2-body interaction

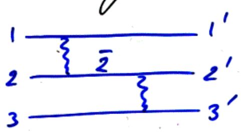

D.S., Sushkov (1997)

$U_c \sim \Delta_2 >> \Delta_3$

- TBRIM

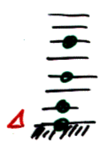

(m) orbitals

(n) fermions

$B = (2m-4)\Delta$

$K \approx \frac{n(n-1)(m-n)(m-n-1)}{4}$

Δ - one-particle spacing

U - two-body matrix element

$\Delta_c = \frac{B}{K}$

$U_c = C\Delta_c = C\frac{B}{K} \approx \frac{2C}{\rho_2 n^2}$ $(\eta = 0.3)$

$C \approx 0.6$ (Jacquod, D.S. (1997))

$C \approx 0.7$ (Åberg (1992))

$C \approx 0.6$ (3d Anderson model)

- Interaction induced thermalization (dynamical) near Fermi level

$\delta E > \Delta\left(\frac{\Delta}{U}\right)^{2/3}, \quad T > \Delta\left(\frac{\Delta}{U}\right)^{1/3}$

| Åberg (1990); Jacquod, D.S. (1997) |

VOLUME 64, NUMBER 26 PHYSICAL REVIEW LETTERS 25 JUNE 1990

Onset of Chaos in Rapidly Rotating Nuclei

Sven Åberg

Joint Institute for Heavy Ion Research, Holifield Heavy Ion Research Facility, Oak Ridge, Tennessee 37831 and Department of Mathematical Physics, Lund Institute of Technology, P.O. Box 118, S-22100 Lund, Sweden[(a)]

(Received 14 August 1989)

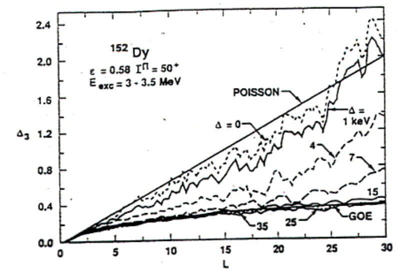

FIG. 3. Δ_3 statistics for different strengths Δ of the two-body force. The calculation has been performed for the superdeformed ^{152}Dy at $I^\pi = 50^+$ for rotational states in the excitation-energy interval 3–3.5 MeV above yrast (about 250 bands).

In conclusion, we have utilized a "realistic" nuclear model to study the onset of chaos in rapidly rotating nuclei. GOE distributions ("quantum chaos") were found to smoothly set in as the strength of the two-body interaction Δ increases to a value around the average level distance between 2p-2h neighbors. Large shell effects in the onset of chaos were found. The dispersion in rotational frequency was found to increase approximately linear in angular momentum, and to be considerably smaller for the superdeformed ^{152}Dy than for the normal-deformed ^{168}Yb. We have addressed the question of how chaotic dynamics is related to a macroscopic quantum observable: It was found that the standard de-

Next we add the residual interaction. The significant part of $H_{res} = H_2 + H_3$ is the two-body part,

$$H_2 = \frac{1}{4}\sum_{m_1 m_2 j_1 j_2} V_2(m_1, m_2, j_1, j_2) \times [a^\dagger_{m_1} a^\dagger_{m_2} a_{j_1} a_{j_2}]_{I=0,\pi=+,\alpha=0}.$$

In the present calculations we assume all matrix elements to have the same absolute value, $V_2 = \pm\Delta$, where Δ is treated as a parameter, and the sign is chosen randomly in order to avoid coherent effects.[8] The three-body force is included in order to account for truncation effects. Its strength is, rather arbitrarily, taken to be $V_3 = \pm 0.001\Delta$. The diagonalization is performed including the lowest 500 states at given spin (thus given signature) and parity. These states cover the energy region 0–3.6 and 0–2.3 MeV above the yrast state in the superdeformed ^{152}Dy and the normal-deformed ^{168}Yb, respectively (for $I^\pi = 50^+$).

diagonalization of Eq. (1) mix over an energy region of unperturbed states Γ_μ that is rather well described by Fermi's "golden rule," $\Gamma_\mu = 2\pi\Delta^2\rho_{2p\text{-}2h}(E_{exc})$; i.e., an increase of the coupling length is obtained either by an increase in Δ or in E_{exc}. In the Fermi-gas model the level density of 2p-2h neighbors is $\rho_{2p\text{-}2h} \propto E_{exc}^{3/2}$.[6] We may thus study the system at the "scaled" energy $s = \Delta^2 \times E_{exc}^{3/2}$,[9] and an increase of the excitation energy can be approximately simulated by an increase in the strength of the two-body interaction Δ in such a way that s is kept constant. The study may then be performed at energy intervals where the level statistics is good. Although this procedure presumably does not account for all possible excitation-energy effects, it is simple and feasible for numerical calculations.

Prog. Part. Nucl. Phys., Vol. 28, pp. 11-47, 1992. 0146-6410/92 $15.00

Quantum Choas and Rotational Damping

S. ÅBERG

Department of Mathematical Physics, Lund Institute of Technology, Box 118, S-221 00 Lund, Sweden

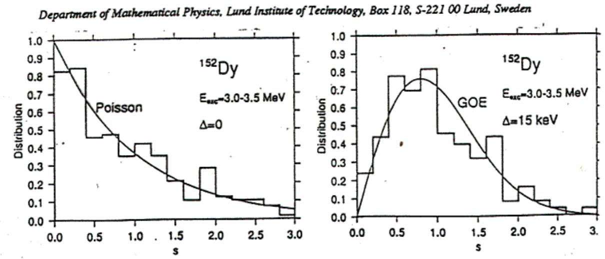

Figure 9: NND for the same cases as considered in fig. 7 but restricted to the excitatic energy interval 3.0 - 3.5 MeV. The solid curves correspond to Poisson and GOE results.

$\frac{U}{\sqrt{3}} \approx \frac{1}{2.5}\Delta_c$

$\Delta \approx (\frac{1}{2} - \frac{1}{3})\,\bar{d}_{2p2h}$.

$C \approx \frac{\sqrt{3}}{2.5} \approx 0.7$

$U_c = 0.6\Delta_c$

Jacquod, D.S. (1997)

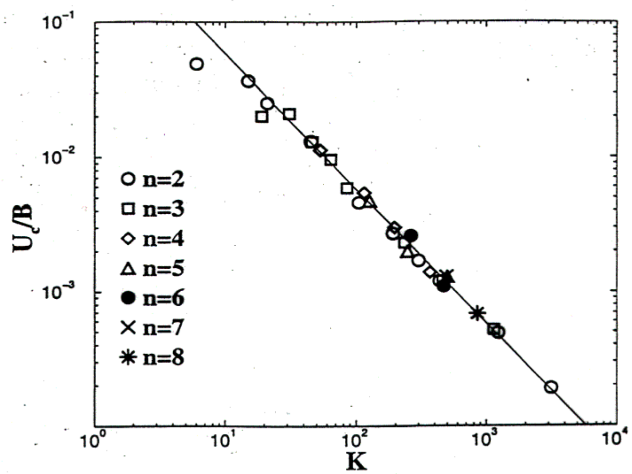

FIG. 2. Dependence of the rescaled critical interaction strength U_c/B, above which $P(s)$ becomes close to the Wigner-Dyson statistics, on the number of directly coupled states K for $4 \le m \le 80$ and $1/40 \le n/m \le 1/2$. The line shows the theory (3) with $C = 0.58$, after [40].

$\eta = 0$ Poisson distribution

$\eta = 1$ Wigner surmise

$\eta(U_c) = 0.3$

Novosibirsk many-body team:

B. Chirikov (Novosibirsk)

V. Flambaum (Sydney)

* F. Izrailev (Puebla)

D. S. (Toulouse)

P. Silvestrov (Novosibirsk) Leiden

O. Sushkov (Sydney)

* V. Zelevinsky (East Lansing)

More about

quant-ph/ of 15 June 2000

Generic model of quantum computer

$$H = \sum_i \Gamma_i \sigma_i^z + \sum_{i<j} J_{ij}\, \sigma_i^x \sigma_j^x$$

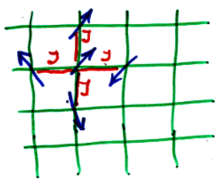

$$\Delta_0 - \frac{\delta}{2} \le \Gamma_i \le \Delta_0 + \frac{\delta}{2}$$

$$0 \le \delta \le \Delta_0 \qquad J_{ij} \in [-J, J]$$

$\delta = \Delta_0$ $\qquad \hbar = 1$

Level spacing statistics

$P_P(s) = e^{-s}$ (Poisson) $J \ll \Delta_0$

$P_W(s) = \frac{\pi s}{2} \exp(-\pi s^2/4)$ (Wigner-Dyson) Random Matrix Theory

$$\eta = \frac{\int_0^{s_0} (P(s) - P_W(s))\,ds}{\int_0^{s_0} (P_P(s) - P_W(s))\,ds}$$

$\eta = 1$ – Poisson

$\eta = 0$ – WD

high energies are important for quantum computer operability

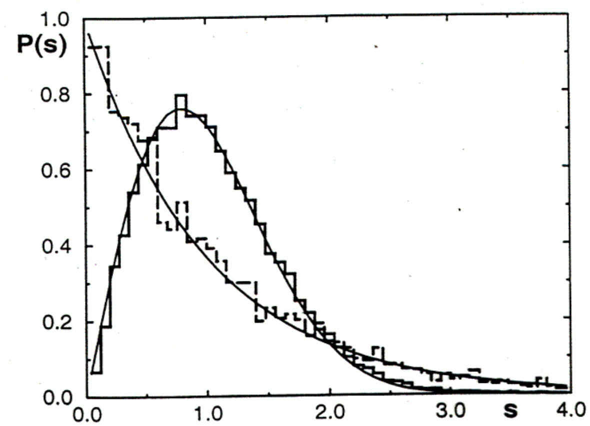

FIG. 1. Transition from Poisson to WD statistics in the model (1) for the states in the middle of the energy band ($\pm 6.25\%$ around the center) for n=12 : $J/\Delta_0 = 0.02, \eta = 1.003$ (dashed line histogram); $J/\Delta_0 = 0.48, \eta = 0.049$ (full line histogram). Full curves show $P_P(s)$ and $P_W(s)$; total statistics $N_S > 2.5 \times 10^4$, number of disorder realizations $N_D = 100$, $\delta = \Delta_0$

Quantum chaos border

for quantum computing

$J > J_c = C_q \frac{\delta}{n}$, $C_q \approx 3$ $\left\| \begin{matrix} B \sim \delta \\ K \sim n \end{matrix} \right\|$

$\Delta_c \sim \frac{\delta}{n}$ Georgeot, D.S. (1999)

Quantum eigenstate entropy

$S_q = - \sum_i W_i \log_2 W_i$

$W_i = | < \psi_i | \phi_m > |^2$

noninteracting multi-qubit eigenstate, $J=0$

quantum computer eigenstate for $J>0$

ideal

$S_q = 0 \rightarrow$ 1 multi-qubit state ($J=0$)

$S_q = 1 \rightarrow$ 2 multi-qubit states

$S_q = n \rightarrow 2^n$ multi-qubit states

$S_q = 1 \Longrightarrow J_{cs}$

$J_{cs} = 0.13 \, J_c \gg \Delta_n$

$n = 16$

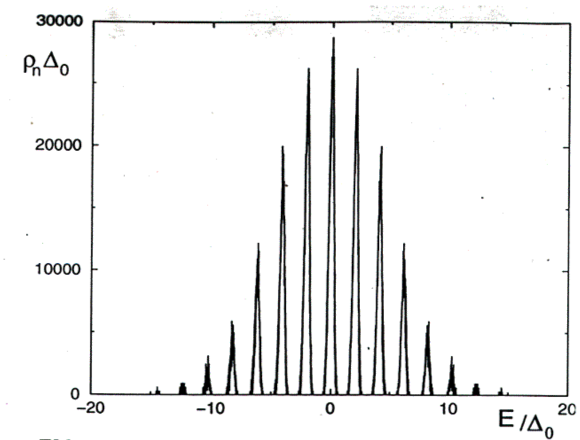

FIG. 1. Density of multi-qubit states of (1) as a function of total system energy E for $J = 0$. Here $n = 16$ and $\delta/\Delta_0 = 0.2$. The two extreme bands at $E/\Delta_0 \approx \pm 16$ contain only one state and are not seen at this scale.

$\Gamma \sim \frac{J^2}{\delta} n$

(small J)

$\Gamma \sim J\sqrt{n}$

(strong $J \gg \delta$)

$n = 15$

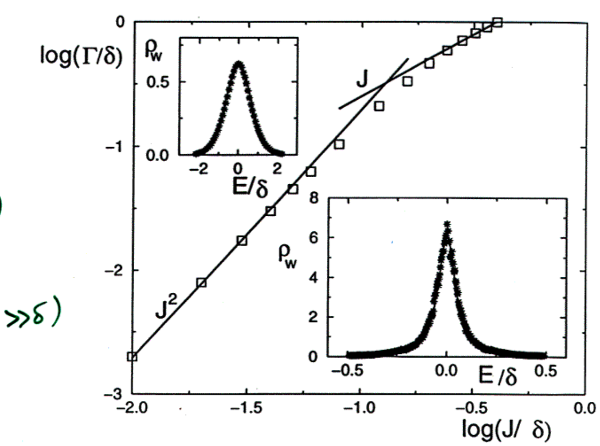

FIG. 8. Dependence of the Breit-Wigner width Γ on the coupling strength J for $n = 15$ for the states in the middle of the energy band. The straight lines show the theoretical dependence (5) with $\Gamma = 1.3J^2n/\delta$ and the strong coupling regime with $\Gamma \sim J$; $N_D = 20$. Lower insert: example of the local density of states ρ_W (3) for $J/\delta = 0.08$; the full line shows the best fit of the Breit-Wigner form (4) with $\Gamma = 0.10\delta$. Upper insert: example of the local density of states ρ_W (3) for $J/\delta = 0.4$; the full line shows the best Gaussian fit of width $\Gamma = 0.64\delta$.

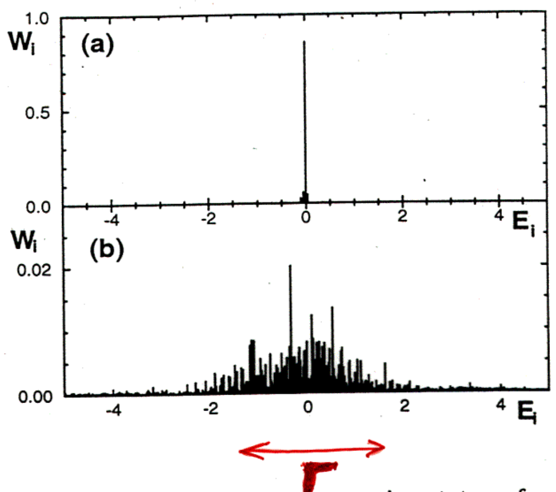

FIG. 3. Two quantum computer eigenstates of model (1) in the basis of noninteracting multi-qubit states, i.e. $W_i = |<\psi_i|\phi>|^2$ as a function of noninteracting multi-qubit energy E_i for $n = 12$ with $J_c/\Delta_0 = 0.273$ (see text): (a) $J/\Delta_0 = 0.02$; (b) $J/\Delta_0 = 0.48$; $\delta = \Delta_0$

Breit - Wigner (spread) width rate

$\Gamma \sim \frac{J^2}{\Delta_c} \sim nJ^2/\delta$

$J_c < J < \delta \leq \Delta_0$

Georgeot, D.S. (1997)

for QC Flambaum (1999)

Georgeot, D.S. (2000)

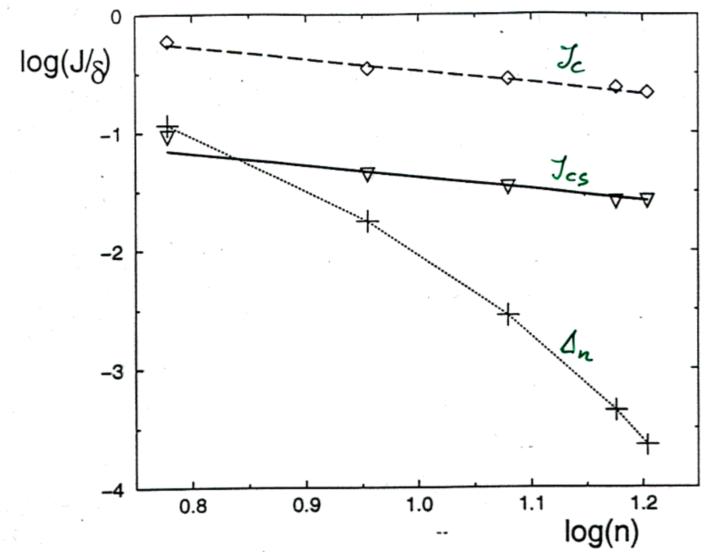

FIG. 5. Dependence of $\log(J_c/\delta)$ (diamonds) and $\log(J_{cs}/\delta)$ (triangles) versus $\log(n)$; the variation of the scaled multi-qubit spacing ($\log(\Delta_n/\delta)$) with $\log(n)$ is shown for comparison (+). Dashed line gives the theoretical formula (7) with $C_q = 3.3$; the solid line is $J_{cs} = 0.41\delta/n$; the dotted curve is drawn to guide the eye for (+). After [25].

$6 \leq n \leq 16$

quantum computer core

Quantum computer melting
induced by interqubit
coupling
Georgeot, DS(1999)

Coupling
$J \uparrow$

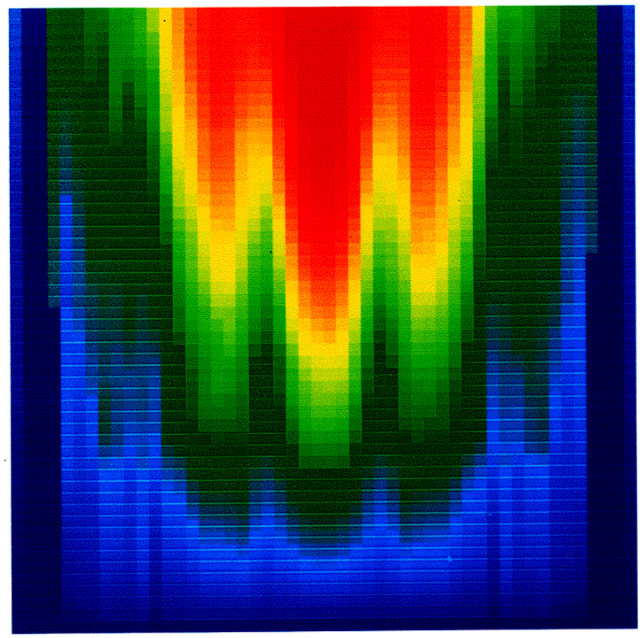

Energy $\overrightarrow{E}$

Quantum eigenstate
entropy color plot

$0 \le S_q \le 11$

$0 \le \frac{J}{\Delta_0} \le 0{,}5$

$0 \le \frac{E}{\Delta_0} \le 2n$

$\delta = \Delta_0$

$n = 12$

$J_c / \Delta_0 = 0.27$

1 random
realization

Time scales for quantum chaos
and decoherence
in quantum computing

Breit-Wigner width $\Gamma \sim J^2 n / \delta$

$J > J_c$

Chaotic time scale

Georgeot, D.S.
Flambaum
(1999)

$\tau_\chi \approx 1/\Gamma$

$\Gamma \sim \frac{J^2 n}{\delta}$ $\quad J < \delta$

$\Gamma \sim J\sqrt{n}$ $\quad J > \delta$

(eigenstates are chaotic
for $\delta = 0$, $J > 0$)

$|\chi(t=0)\rangle = |\psi_{i_0}\rangle$

$F_{i i_0}(t) = |\langle \psi_i | \chi(t) \rangle|^2$

Quantum entropy

$S(t) = -\sum_i F_{i i_0}(t) \log_2 F_{i i_0}(t)$

Exponentially many states
are mixed after τ_χ

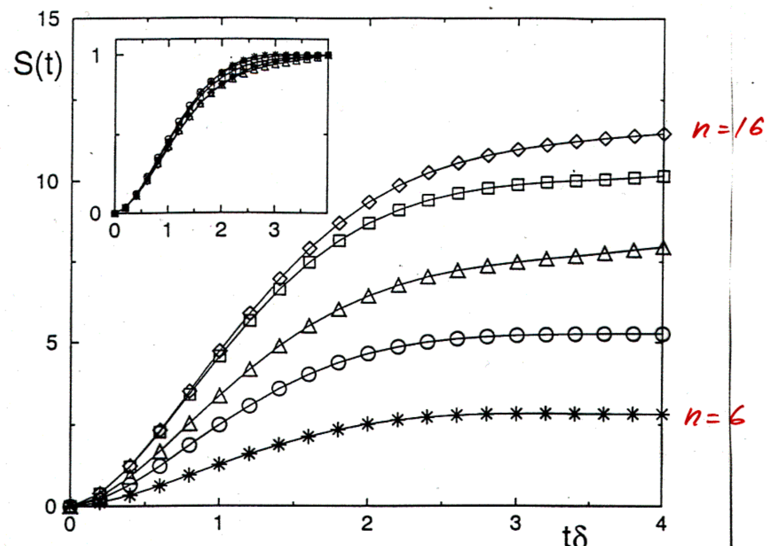

FIG. 7. Time-dependence of the quantum entropy $S(t)$ for $J/\delta = 0.4 > J_c/\delta$ and $n = 16$ (diamonds), $n = 15$ (squares), $n = 12$ (triangles), $n = 9$ (circles), $n = 6$ (*). Average is made over 200 initial states i_0 randomly chosen in the central band. Insert shows the same curves normalized to their maximal value. After [25].

quantum entropy growth

G. Benenti, G. Casati, D. S. (2001)

Dynamical thermalization in the quantum computer core

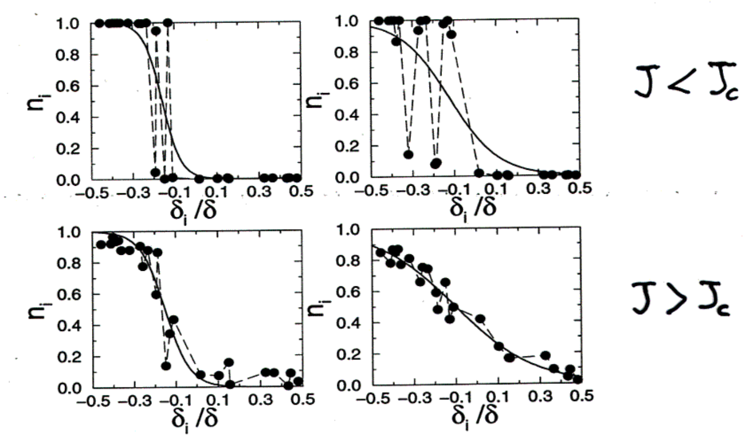

Distribution of the **occupation numbers** n_i as a function of the qubit detunings δ_i, for one random realization and **one eigenstate** $m = 5/100$ (left/right). Solid line shows the Fermi-Dirac distribution with effective temperature T_{FD}.

Number of qubits $n = 24$

LANL

First quantum paper of the Millennium III

http://arXiv.org/abs/quant-ph/0101004

Quantum Physics, abstract
quant-ph/0101004

From: SHEPELYANSKI Dimitrii < dima@irsamc.ups-tlse.fr>
Date: Mon, 1 Jan 2001 00:01:12 GMT (103kb)

Quantum Computing of Classical Chaos:
Smile of the Arnold-Schrödinger Cat

Authors: B.Georgeot, D.L.Shepelyansky (CNRS,Toulouse)
Comments: revtex, 4 pages, 4 figures
Subj-class: Quantum Physics; Chaotic Dynamics

We show on the example of the Arnold cat map that classical chaotic systems can be simulated with exponential efficiency on a quantum computer. Although classical computer errors grow exponentially with time, the quantum algorithm with moderate imperfections is able to simulate accurately the unstable chaotic classical dynamics for long times. The algorithm can be easily implemented on systems of a few qubits.

Paper: Source (103kb), PostScript, or Other formats

1

Quantum computing
of classical chaos:
smile of
Arnold-Schrödinger cat

$$\bar{y} = y + x \mod(1)$$
$$\bar{x} = \bar{y} + x \mod(1)$$

time inversion test $(t = t_r)$
discretization $N \times N$, $N = 2^{n_q}$

x_i, y_j : $x_i = i/N$, $y_j = j/N$
$0 \le i, j \le N-1$

$$\psi(t=0) = \sum_{i,j} a_{ij} |x_i\rangle |y_j\rangle |0\rangle$$
$a_{ij} = 0$ or $1/\sqrt{N_d}$ $\quad N_d = O(N^2)$

Quantum computer iteration involves

- 3 registers with $3n_q - 1$ qubits $N = 2^{n_q}$
- $8n_q - 12$ Toffoli gates
  $8n_q - 10$ controlled-not gates

PHYSICAL REVIEW A VOLUME 54, NUMBER 1 JULY 1996

Quantum networks for elementary arithmetic operations

Vlatko Vedral,* Adriano Barenco, and Artur Ekert
Clarendon Laboratory, Department of Physics, University of Oxford, Oxford OX1 3PU, United Kingdom

(Received 3 November 1995)

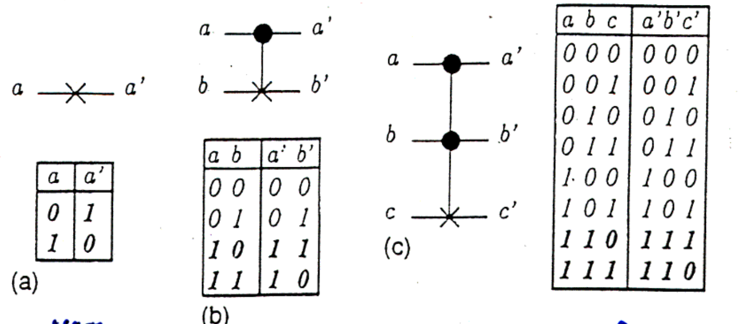

a	a'
0	1
1	0

a b	a' b'
0 0	0 0
0 1	0 1
1 0	1 1
1 1	1 0

a b c	a' b' c'
0 0 0	0 0 0
0 0 1	0 0 1
0 1 0	0 1 0
0 1 1	0 1 1
1 0 0	1 0 0
1 0 1	1 0 1
1 1 0	1 1 1
1 1 1	1 1 0

NOT control-NOT Toffoli

FIG. 1. Truth tables and graphical representations of the elementary quantum gates used for the construction of more complicated quantum networks. The control qubits are graphically represented by a dot, the target qubits by a cross. (a) NOT operation. (b) control-NOT. This gate can be seen as a "copy operation" in the sense that a target qubit (b) initially in the state 0 will be after the action of the gate in the same state as the control qubit. (c) Toffoli gate. This gate can also be seen as a control-control-NOT: the target bit (c) undergoes a NOT operation only when the two controls (a and b) are in state 1.

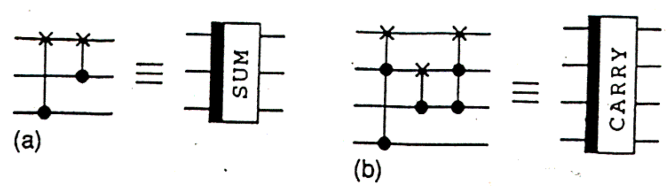

FIG. 3. Basic carry and sum operations for the plain addition network. (a) the carry operation (note that the carry operation perturbs the state of the qubit b). (b) the sum operation.

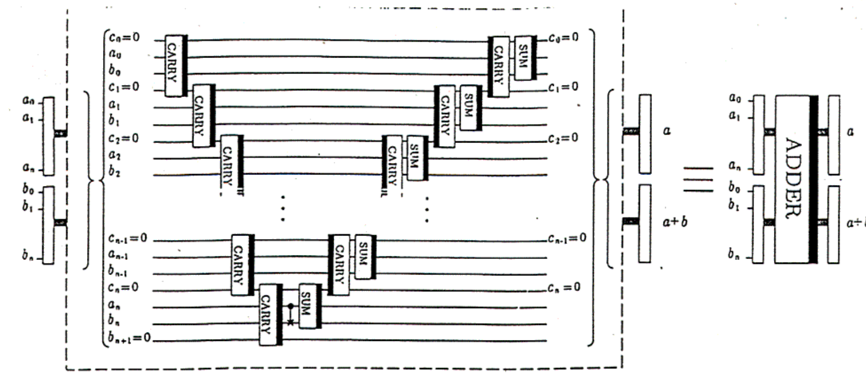

FIG. 2. Plain adder network. In the first step, all the carries are calculated until the last carry gives the most significant digit of the resu[lt]. Then all these operations apart from the last one are undone in reverse order, and the sum of the digits is performed correspondingly. No[te] the position of a thick black bar on the right- or left-hand side of basic carry and sum networks. A network with a bar on the left sid[e] represents the reversed sequence of elementary gates embedded in the same network with the bar on [the] right side.

$16\, n_q$ quantum gates

vs.

$O(2^{2n_q})$ classical operations

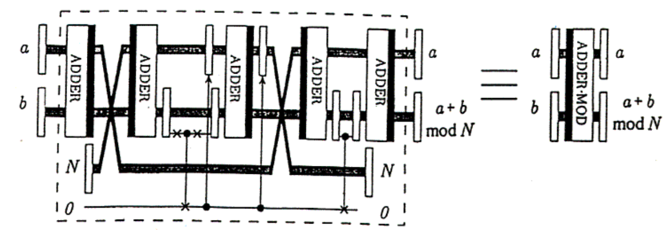

FIG. 4. Adder modulo N. The first and the second network add a and b together and then subtract N. The overflow is recorded into th[e t]emporary qubit $|t\rangle$. The next network calculates $(a+b)\bmod N$. At this stage we have extra information about the value of the overflo[w s]tored in $|t\rangle$. The last two blocks restore $|t\rangle$ to $|0\rangle$. The arrow before the third plain adder means that the first register is set to $|0\rangle$ if the valu[e o]f the temporary qubit $|t\rangle$ is 1 and is otherwise left unchanged (this can be easily done with control-NOT gates, as we know that the firs[t r]egister is in the state $|N\rangle$). The arrow after the third plain adder resets the first register to its original value (here $|N\rangle$). The significance o[f t]he thick black bars is explained in the caption of Fig. 2.

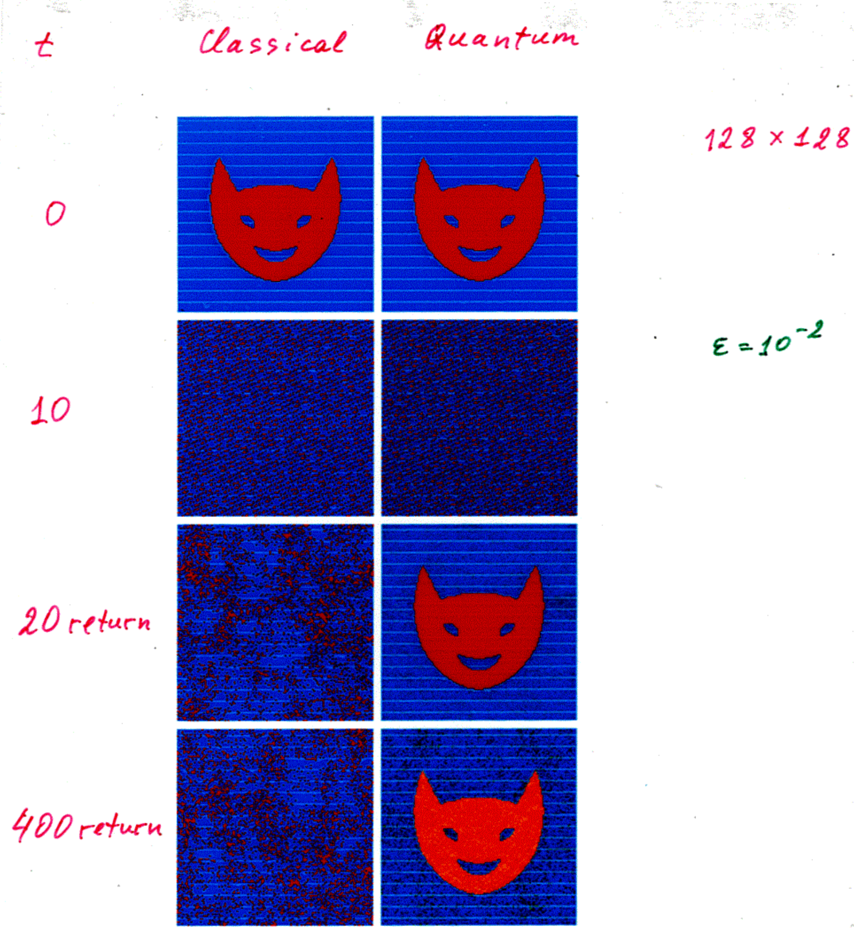

Figure 1: Dynamics of Arnold-Schrödinger cat simulated on a classical (left) and quantum computer (right), on a 128 × 128 lattice. Upper row: initial distribution; second row: distributions after 10 iterations; third row: distributions at $t_{2r} = 20$, with time inversion made at $t_r = 10$; bottom row: distributions at $t_{2r} = 400$, with time inversion made at $t_r = 200$. Left: inversion is done with classical error of one cell size ($\epsilon = 1/128$) at $t = t_r$ only; right: all quantum gates operate with quantum errors of amplitude $\epsilon = 0.01$; color from blue to red gives the probability $|a_{ij}|^2$; $n_q = 7$.

in total 20 qubits

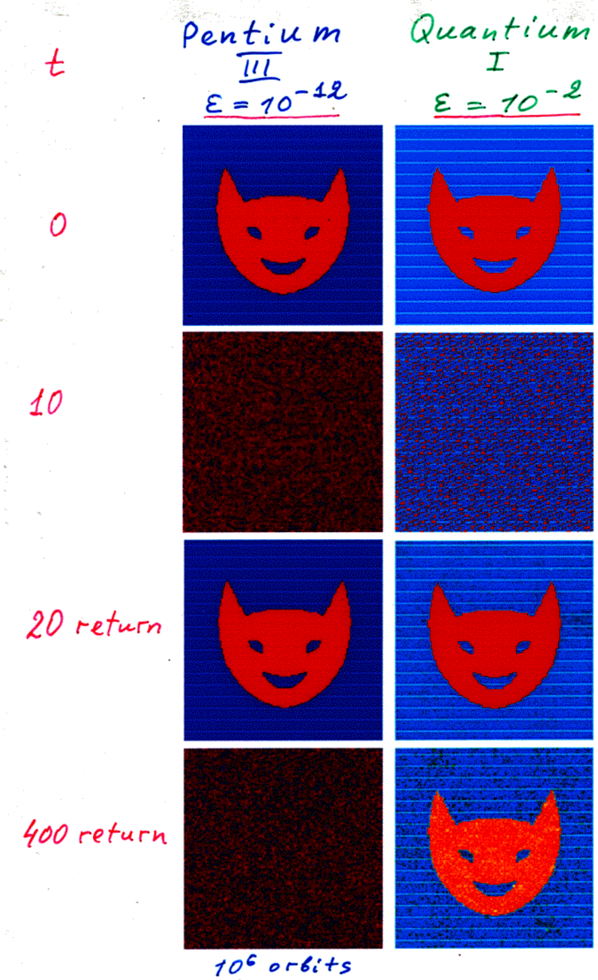

Figure 1: Dynamics of Arnold-Schrödinger cat simulated on Pentium III (left) and Quantium I (right). Image is shown on a 128 × 128 lattice. Upper row: initial distribution; second row: distributions after 10 iterations; third row: distributions at $t_{2r} = 20$, with time inversion made at $t_r = 10$; bottom row: distributions at $t_{2r} = 400$, with time inversion made at $t_r = 200$. Left: inversion is done with classical error $\epsilon = 10^{-12}$ at $t = t_r$ only; right: all quantum gates operate with quantum errors of amplitude $\epsilon = 0.01$; color from blue to red gives the probability $|a_{ij}|^2$; $n_q = 7$. Quantium I operates with 20 qubits.

Cat fidelity f

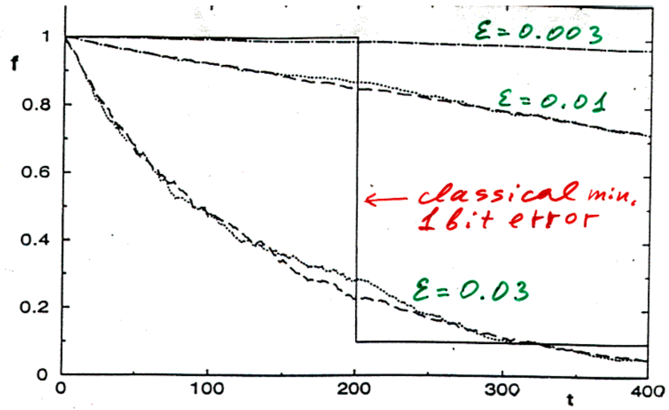

FIG. 2. Quantum fidelity f of Arnold-Schrödinger cat as a function of time t for quantum errors $\epsilon = 0.003, 0.01, 0.03$ (dashed and dotted curves from top to bottom respectively). Initial state: cat's smile as in Fig. 1 (dashed curves) and line $x = 1/2$ (dotted curves). Full curve shows the drop of fidelity when a minimal classical error is done at $t = 200$ (see text).

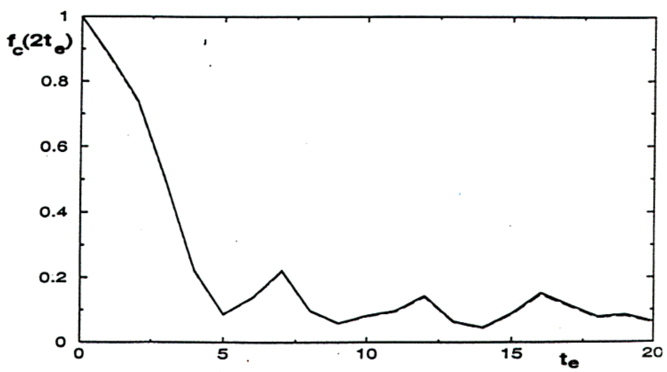

FIG. 3. Classical fidelity $f_c(2t_e)$ vs. time t_e when the minimal classical error ($\epsilon = 1/128$) is made (full curve). Dashed curve shows the same f_c obtained by the quantum computer with imperfections of amplitude $\epsilon = 0.01$ (see text).

$f(t) = |\langle \psi_\varepsilon(t) | \psi_0(t) \rangle|^2$

$\psi_0(t)$ – exact ; $\psi_\varepsilon(t)$ – with imperfections

t_f

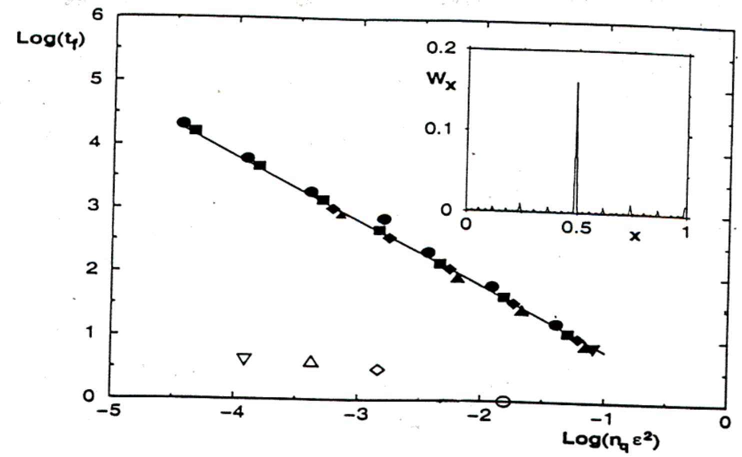

FIG. 4. Fidelity time scale t_f as a function of $\epsilon^2 n_q$: $n_q = 4$ (circles), 5 (squares), (diamonds), 7 (triangles up), 8 (triangles down)); filled symbols are for quantum errors ($0.003 \leq \epsilon \leq 0.1$), open ones are for classical errors ($0.003 < \epsilon < 0.1$); the full line gives $t_f = 0.63/(\epsilon^2 n_q)$. Inset: probability distribution W_x in $|x>$ at the moment of return $t_{2r} = 400$ for time inversion at $t_r = 200$, and quantum imperfections $\epsilon = 0.03$, for $n_q = 7$ with $x = 1/2$ at $t = 0$.

$f(t_f) = 0.5$

$t_f \approx \dfrac{0.63}{\varepsilon^2 n_q}$ — quantum error ε

$\varepsilon^2 n_q t_f \sim 0.5$

$t_f \approx 1.4 \ln(1/\varepsilon)$ — classical error ε

Boltzmann-Loschmidt controversy

A legend tells that once Loschmidt asked Boltzmann on what happens to his statistical theory if one reverses the velocity of all particles, so that, due to the reversibility of Newton's equations, they return from the equilibrium to a nonequilibrium initial state. Boltzmann only replied "then go and invert them"

(from Mayer and Goeppert-Mayer *Statistical mechanics*, Wiley & Sons, N.Y. 1976)

submitted to Science

Quantum computer turning the arrow of time

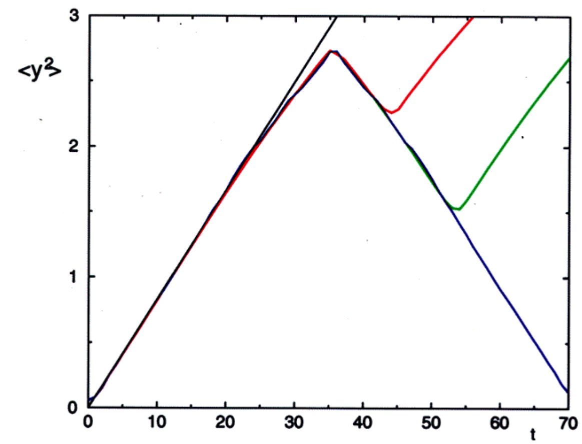

Figure 1: Diffusive growth of the second moment $< y^2 >$ of the distribution $w(y,t)$ generated by the Arnold cat map with $L = 8$, simulated on a classical (Pentium III) and quantum ("Quantium I") computers. At $t = t_r = 35$ Maxwell's demon inverts all velocities. For Pentium III inversion is done with precision $\epsilon = 10^{-4}$ (red line) and $\epsilon = 10^{-8}$ (green line); 10^6 orbits are simulated, initially distributed inside initial distribution. For Quantium I, the computation is done with 26 qubits ($n_q = 7, n_{q'} = 10$)(blue line); each quantum gate operates with imperfections of amplitude $\epsilon = 0.01$ (unitary rotation on a random angle of this amplitude). The black straight line shows the theoretical macroscopic diffusion with $D = 1/12$.

$\bar{y} = y + x \pmod{L}, \quad \bar{x} = x + \bar{y} \pmod{1}$

Thermodynamical distribution

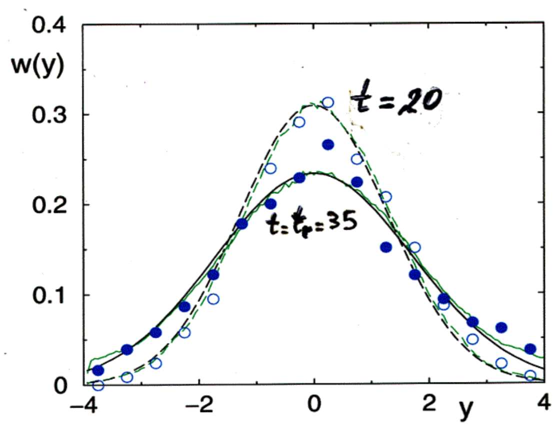

Pentium III with 10^6 orbits

Quantum I with 26 qubits (lattice 128×1024)

theoretical $w_g(y)$

$\Rightarrow$ Convergence to thermodynamical distribution

Classical and quantum errors

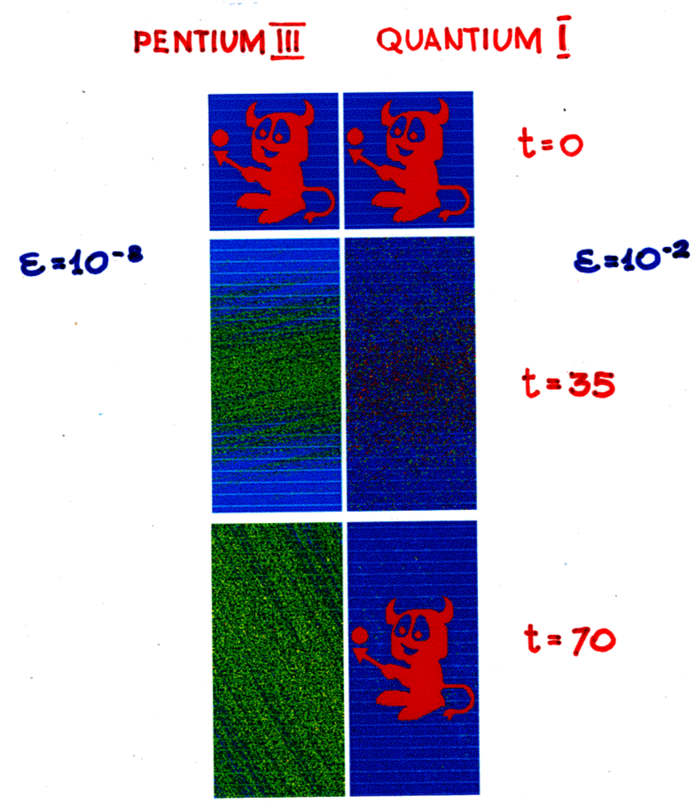

Scaling of quantum errors

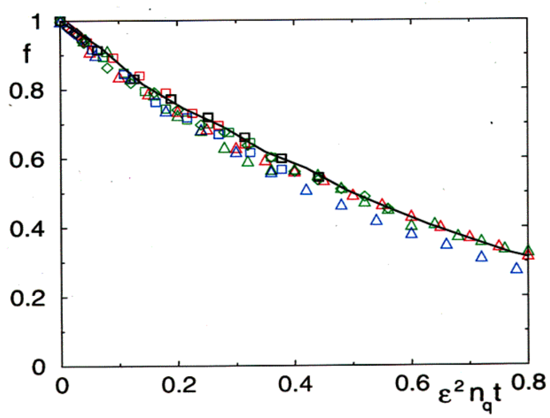

Universality of fidelity $f = |<\psi_\epsilon|\psi_0>|^2$ as a function of $tn\epsilon^2$ for Quantum I

$4 \le n \le 7; \quad 10^{-2} \le \epsilon \le 10^{-1}$

$$\boxed{t_f \approx 0.5/(n\epsilon^2)}$$

n number of qubits, ϵ quantum errors

t_f defined by $f(t_f) = 0.5$

Macroscopic system

- $N_d = 6.022 \times 10^{23}$ (Avogadro's number) requires only 125 qubits for $L = 8$
- In this case, if $\epsilon = 0.01$, quantum errors will be small up to a time $t \approx 150$
- Boltzmann's demand can be performed !
- Applications in cryptography?

God does not play dice

Albert Einstein

he simply
control-not-s them.